

strength groups namely G10, G25, G50 and G80 is shown in Table 1. In order to ensure statistical homogeneity of the specimens, all the concrete cylinders were extracted from larger existing concrete blocks measuring 2000 x 300 x 350 mm using a coring machine. The cores were then cut to lengths of 300 mm and both ends of each core were ground using a special surface grinder, ensuring that the ends are flat and perpendicular to the long axis of the specimen. In order to ensure the consistency of concrete specimens, prior to testing, all specimens were moist-cured for at least one week to ensure that they are fully saturated before testing.

Test equipment

Triaxial test apparatus comprise mainly of the following components: a) Rockcell Model 10 Triaxial Cell; b) Instron Load Frame; c) Confining Pressure System and d) Axial and Circumferential Deformation Device. The triaxial cell is designed to withstand a maximum lateral confining pressure of 70 MPa and the maximum loading capacity of the Instron loading frame is 2000 kN. The confining pressure system is servo-hydraulic and close-loop control. It is totally independent of the axial loading system and consists of a hydraulic pressure supply and a hydraulic pressure intensifier. The pressure intensifier is used to provide hydraulic pressure in the triaxial cell. The close-loop command and feedback control for the pressure system is managed by Instron digital controller.

The concrete specimen was first aligned with the lower and upper platen and then jacketed with a heat-shrink membrane to prevent hydraulic oil from penetrating the concrete during the test. Two LVDTs with 2.5 mm maximum stroke were used to measure axial deformation of the specimen and a circumferential LVDT, with 2.5 mm maximum stroke, was used to measure lateral deformation of the specimen. The axial LVDTs with gauge length of 100 mm were positioned in the central portion of the specimen. The circumferential LVDT was placed around the specimen at the midheight of the specimen. (Fig. 2)

Test procedure

Prior to testing, a load of about 10% of the uniaxial failure load was applied to the specimen to minimize the initial take-up reading due to the presence of any minute gaps at the interfaces. The load was gradually reduced to zero and similarly the confining pressure was adjusted to zero. For safety purpose, the maximum limit for the failure load was pre-set to prevent any sudden changes to occur during the loading. All the test readings such as load, pressure, position, time as well as axial and radial displacement were automatically logged by an Instron test programme named MAX. For triaxial tests with active confining stress, the axial compressive stress, σ_1 and the confining stress ($\sigma_2 = \sigma_3$) were initially increased up to a predetermined value ($\sigma_1 = \sigma_2 = \sigma_3$), and thereafter the confining stress was kept constant and the axial load was further increase until the specimen fails ($\sigma_1 > \sigma_2 = \sigma_3$).

Before concrete reaches the unstable fracture stage i.e. at about 70% to 80% of the peak stress, the circumferential deformation is low and the loading can be executed using the axial strain for control. Beyond that stage, particularly for unconfined concrete but less so for confined one, the circumferential deformation increases rapidly and uncontrollably. Shown in Fig. 3 is a relationship of ε_1 (axial strain) and ε_2 (circumferential strain) versus time under single channel control of ε_1 . It is to be noted that ε_2 increases rapidly when the axial stress is close to the peak stress if the axial loading rate is held constant. This phenomenon makes the use of axial strain an unstable control parameter which will result in a sudden brittle failure in high strength concrete. Moreover, the response of the confining pressure may not be fast enough to keep up with the rate of circumferential deformation.

Cross compensation control - In order to have a more controllable failure, the loading of the specimen has to be changed to one based on the circumferential strain¹⁰. Therefore, a cross compensation control method is used in this study. In conventional testing, the servo feedback comes from single channel which can be either the axial strain or the circumferential strain. Cross compensation control is based on the feedback from the combination of two signals. Fig. 4 reveals the strains versus time relationships under cross compensation control. The feedback consists of two signals in the combination of $(a\varepsilon_1 + b\varepsilon_2)$, where a, b are compensation factors and ε_1 , ε_2 are feedback signals. It should be noted that at the beginning of loading, the feedback is axial strain dominant and the loading rate is high. When concrete is approaching its peak stress, the loading rate is slowed down when the feedback is gradually transferred to circumferential strain dominant. Thus, it is possible to achieve a less brittle failure in order to obtain a complete stress-strain curve when the feedback signal is gradually dominated by the circumferential strain.

In this investigation, four groups of concrete specimens termed as G10, G25, G50 and G80 were tested. The uniaxial compressive strength of these groups was 10.35, 27.2, 51.8 and 77.46 MPa respectively. At least 3 specimens were tested to determine the uniaxial compressive strength for each group. Stress-strain relationships of G10 and G80 concrete under active confinement of various confining stresses are shown in Fig. 5 and 6 respectively.

EXPERIMENTAL RESULTS AND DISCUSSIONS

As expected, the results show that the peak stress level is dependent on the confinement level. The higher the confinement, the higher the peak stress and the corresponding strain the concrete can achieve. The test results are summarised in Table 2.

Proposed failure envelope for concrete

The general shape of failure envelope of concrete is usually described as open-ended and has a convex polar figure which has threefold symmetry with respect to the hydrostatic axis. The failure curve is nearly triangular for tensile and small compressive stresses, and becomes more circular corresponding to the increasing value of hydrostatic

pressure. Among the failure criteria proposed in the past, William and Warnke’s “five-parameter” model⁴ reflects the principal features of the triaxial failure surface of concrete. In this study, their model was adopted to define the failure envelope for concrete under triaxial stress state. The ultimate failure condition for concrete can be defined in terms of compressive and tensile surfaces, which are functions of the octahedral normal stress . The tensile and compressive meridians are expressed as follows:

$$\frac{\tau_o}{f_c'} = a_0 + a_1 \frac{\sigma_o}{f_c'} + a_2 \left(\frac{\sigma_o}{f_c'}\right)^2 \quad \text{at } \theta = 0^\circ \quad \text{Tensile meridian}$$

$$\frac{\tau_o}{f_c'} = b_0 + b_1 \frac{\sigma_o}{f_c'} + b_2 \left(\frac{\sigma_o}{f_c'}\right)^2 \quad \text{at } \theta = 60^\circ \quad \text{Compressive meridian}$$

The coefficients of the equations are chosen so that the surfaces pass through a set of control points given by the “five parameters”, namely the unconfined concrete compressive strength, the tensile strength, the equal biaxial compressive strength and a defined point on each of the two surface meridians. For the compressive meridian, the number of parameters is reduced to three. These three parameters can be derived by regression of the experimental results. For the triaxial test condition, the equation of compressive meridian can be written as follows:

$$\bar{\sigma}_o = \frac{\sigma_1 + \sigma_2 + \sigma_3}{3f_c'} = -\frac{f_o}{3f_c'} - \frac{2f_r}{3f_c'} \tag{1}$$

$$\bar{\tau}_o = \frac{1}{3f_c'} \sqrt{(\sigma_1 - \sigma_2)^2 + (\sigma_2 - \sigma_3)^2 + (\sigma_3 - \sigma_1)^2} = -\sqrt{2} \left(\bar{\sigma}_o + \frac{f_r}{f_c'} \right) \tag{2}$$

For triaxial case $\sigma_1 = \sigma_2 = -f_r$, $\theta = 60^\circ$;

$$\bar{\tau}_o = b_0 + b_1(\bar{\sigma}_o) + b_2(\bar{\sigma}_o)^2 \tag{3}$$

Substituting Eq.2 into Eq.3, produces

$$b_2(\bar{\sigma}_o)^2 + (b_1 + \sqrt{2})(\bar{\sigma}_o) + \left(b_0 + \frac{\sqrt{2}f_r}{f_c'} \right) = 0 \tag{4}$$

Solving Eq.4 and incorporating Eq. 1, the result is

$$\frac{f_o}{f_c'} = \frac{3(b_1 + \sqrt{2})}{2b_2} + \sqrt{\left(\frac{3(b_1 + \sqrt{2})}{2b_2} \right)^2 - \frac{9b_0}{b_2} - \frac{9\sqrt{2}}{b_2} \frac{f_r}{f_c'} - \frac{2f_r}{f_c'}} \tag{5}$$

By regression of experimental data, for concrete uniaxial strength within 10.35~77.46 MPa, the three parameters can be defined as: $b_0 = 0.19$, $b_1 = -0.8725$ and $b_2 = -0.087$. Therefore, Eq.5 can be transformed into:

$$f_o = f_c' \left(-9.338 + 10.338 \sqrt{1 + 1.368 \frac{f_r}{f_c'} - 2 \frac{f_r}{f_c'}} \right) \quad (6)$$

where f_o = peak strength of confined concrete; f_r = lateral confining pressure on concrete; f_c' = Standard concrete cylinder strength.

The proposed failure envelope was compared with experimental results as shown in Fig. 7. Based on experimental observation, it should be noted that for concrete under active confinement, concrete with different uniaxial compressive strength will result in different failure envelopes. However, the differences between these envelopes are insignificant especially for normal and high strength concrete. In this study, the proposed failure envelope is suitable for low, normal and high-strength concrete. Comparisons were also made between active and passive confinement with different lateral stiffness. It was found that the failure envelope under passive confinement is slightly different from that of active confinement for the same grade of concrete (Figure 8); the higher the stiffness of lateral confinement, the closer the failure envelope to that of active confinement¹¹. This suggests that different stress paths produce different failure envelopes but the difference is minor. Hence the proposed failure envelope can still represent all the data with reasonable accuracy. It was observed that the proposed failure envelope also has a close fit with the test results tested by other researchers (Figures 9 and 10) for a wide range of concrete uniaxial compressive strength of up to 119 MPa.

In Fig.11, proposed failure envelope is compared with failure envelopes proposed by other researchers. It is interesting to find that the proposed failure envelope is close to failure surfaces proposed by Hobbs² and Kotsovos³. Up to about lateral stress ratio of 0.4, the linear relationship is more conservative but beyond that, Mander's model¹² produces a lower strength boundary and Setunge's model⁵ gives an upper boundary for all lateral stress ratio. Moreover, all of these models proposed are assumed to be stress path independent. The differences between these models may be caused by different experimental results for different aspect ratio of specimen and various test conditions.

CONCLUDING REMARKS

In this paper, the results of experimental work on the strength properties of low, normal and high strength concrete were presented. A cross compensation control method was adopted to avoid sudden brittle failure of concrete especially for high-strength concrete during the test. The failure surface of concrete under lateral confinement was determined through regression analysis of the experimental data. The following conclusions are drawn based on the findings of this study:

1. The strength and ductility of concrete under lateral confinement are influenced by the lateral confining stress. The higher the confining stress, the higher the peak stress and peak strain concrete can achieve.
2. For concrete under active confinement, different concrete uniaxial strength will result in different failure envelopes. However, the differences between these envelopes are insignificant especially for normal and high-strength concrete. The differences caused by stress-path on failure envelope were also found to be small. It is reasonable to establish a single failure criterion to describe the strength property for concrete under lateral confinement.
3. The proposed failure envelope is suitable for low, normal and high-strength concrete, even for very high-strength concrete with uniaxial compressive strength up to about 120 MPa.

REFERENCES

1. Richart, F. E., Brantzaeg, A., and Brown, R. L., "The Failure of Plain and Spirally Reinforced Columns in Compression", University of Illinois Engineering Experimental Station, Bulletin No. 190, 1929.
2. Hobbs, D. W., Pomeroy C. D., and Newman, J. B., "Design Stresses for Concrete Structures Subjected to Multi-axial Stresses", *The Structural Engineer*, No. 4, Vol. 55, April 1974.
3. Kotsovos, M. D., "A Generalized Constitutive Model of Concrete Based on Fundamental Material Properties", Civil Engineering Department, Imperial College of Science and Technology, London, August 1980.
4. William, K. J., and Warnke, E. P., "Constitutive Models for the Triaxial Behaviour of Concrete", Seminar on concrete structures subjected to triaxial stress, Istituto Sperimentale Modelie Structure (ISMES), Bergamo, Italy, 1974.
5. S. Setunge, M. M. Attard, and P. LeP. Darvall., "Ultimate Strength Of Confined Very High-Strength Concrete", *ACI Structural Journal*, V. 90, No. 6, November-December 1993.
6. J. Xie et al., "Mechanical Properties of Three High-Strength Concrete Containing Silica Fume", *ACI Material Journal*, 1995, 92(2), pp. 135-145.
7. Imran and S. J. Pantazopoulou, "Experimental Study of Plain Concrete under Triaxial Stress", *ACI Material Journal*, V. 93, No. 6, Nov-Dec 1996, pp. 589-601.
8. Tan, T.H., Cheong, H.K., An apparatus for testing concrete under active and passive confining stress, *Strength Theory, Application, Development & Prospect for 21st Century*, China, 1998, pp 557 – 567.
9. Kotsovos, M. D., "A Mathematical Description of the Strength Properties of Concrete Under Generalized Stress", *Magazine of Concrete Research*, Vol. 81, No. 108, September 1979, pp. 151-157.

242 Tan and Sun

10. D. C. Jansen et al. "Stress-strain Results of Concrete from Circumferential Strain Feedback Control Testing", *ACI Material Journal*, 1995, 92(4), pp. 419-428.

11. Sun Xin, Tan, T.H., Irawan, P., Effect of Stress-Path on the Failure of Concrete under Triaxial Stress State, *Proceedings of the Seventh East Asia-Pacific Conference on Structural Engineering and Construction*, Japan, 1999, pp 1437 - 1442.

12. Mander, J. B., Priestley, M. J. N., and Park, R., "Observed Stress-Strain Behaviour of Confined Concrete", *Journal of Structural Engineering*, Vol. 114, No. 8. August, 1988, pp. 1827-1849

Table 1. Mix design of concrete

Grade of concrete	G10	G25	G50	G80
Compressive strength at 3 months (MPa)	10.35	27.2	51.8	77.46
Slump (mm)	100	100	150~200	200 ± 25
Cement (kg)	230	345	450	540
Silica fume (kg)	0	0	0	60
Water (kg)	190	190	160	145
Aggregate (kg)	1020	1000	1000	1050
Sand (kg)	870	810	760	595
Water/cement ratio	0.82	0.55	0.36	0.24

Table 2. Test results of concrete under active confinement

Spec. Number	f_c (Mpa)	D (mm)	H (mm)	Max σ_2 (MPa)	Failure load (KN)	Peak σ_1 (MPa)	Peak ϵ_1 (mm/m)
G10A-1	10.35	100.9	299.4	0	83.55	10.45	1.07
G10A-2	10.35	101.7	301.4	0	89.55	11.02	0.87
G10A-3	10.35	100.9	300.6	1.875	105.89	14.57	2.51
G10A-4	10.35	101.0	300.6	1.875	115.99	15.8	3.23
G10A-5	10.35	101.0	300.3	7.5	114.11	19.56	2.10
G10A-6	10.35	101.0	299.4	7.5	114.04	19.59	2.05
G10A-7	10.35	100.8	300.5	12.5	135.64	25.85	3.90
G10A-8	10.35	100.8	301.3	12.5	127.35	24.81	2.97
G25A-1	27.2	100.1	299.1	0	196.85	25.10	1.63
G25A-2	27.2	101.5	298.9	0	215.68	26.67	2.0
G25A-3	27.2	100.3	299.0	1.875	275.59	36.22	3.0
G25A-4	27.2	100.3	298.0	1.875	271.44	35.69	2.89
G25A-5	27.2	100.6	299.6	7.5	356.05	50.13	4.35
G25A-6	27.2	100.5	300.1	7.5	334.28	47.48	5.73
G25A-7	27.2	101.5	299.6	15.0	495.97	72.05	7.44
G25A-8	27.2	101.5	299.6	15.0	451.96	66.61	8.02
G50A-1	51.8	100.5	299.4	0	393.69	49.63	2.27
G50A-2	51.8	100.5	299.8	0	428.68	54.04	2.48
G50A-3	51.8	100.0	299.7	1.875	498.45	64.79	3.29
G50A-4	51.8	100.0	299.5	1.875	507.66	65.97	3.86
G50A-5	51.8	100.0	300.3	7.5	638.48	86.61	4.56
G50A-6	51.8	100.0	299.3	7.5	619.55	84.2	4.89
G50A-7	51.8	100.7	300.6	12.5	720.10	99.27	4.92
G50A-8	51.8	100.9	300.0	12.5	755.16	103.29	6.62
G80A-1	77.46	101.3	300.2	0	614.59	76.26	2.61
G80A-2	77.46	101.5	300.0	0	646.27	79.87	3.03
G80A-3	77.46	101.1	299.7	1.875	729.42	92.2	4.08
G80A-4	77.46	100.9	299.5	1.875	744.95	94.51	3.90
G80A-5	77.46	100.8	300.8	7.5	963.74	126.09	5.72
G80A-6	77.46	100.3	301.0	7.5	942.39	124.59	5.16
G80A-7	77.46	100.9	299.9	12.5	1033.47	138.1	6.12
G80A-8	77.46	100.6	300.3	12.5	988.46	133.21	6.20

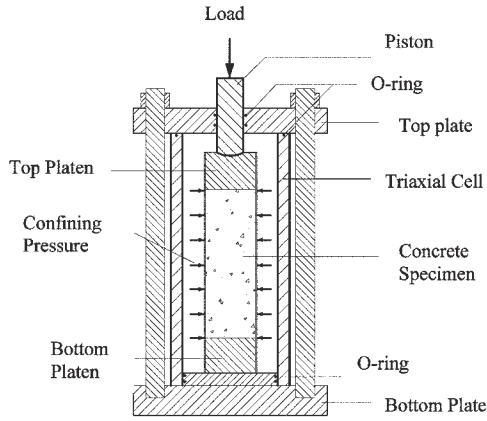


Figure 1 – Rockcell Model 10 triaxial cell



Figure 2 – Setup of specimen

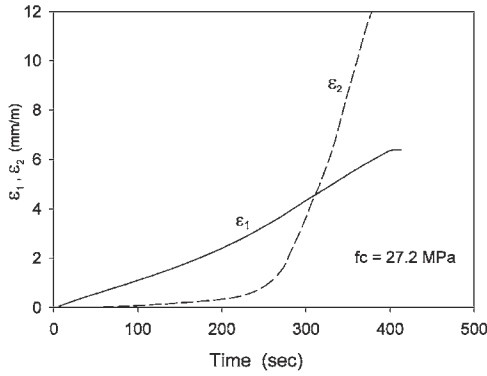


Figure 3 – Single channel control

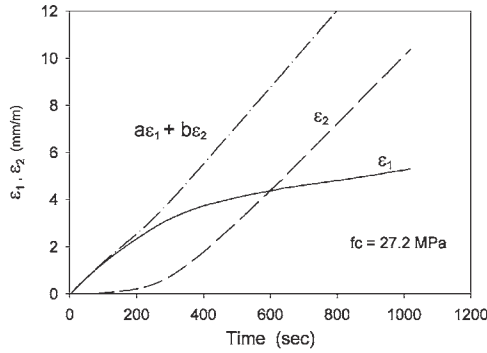


Figure 4 – Cross compensation control

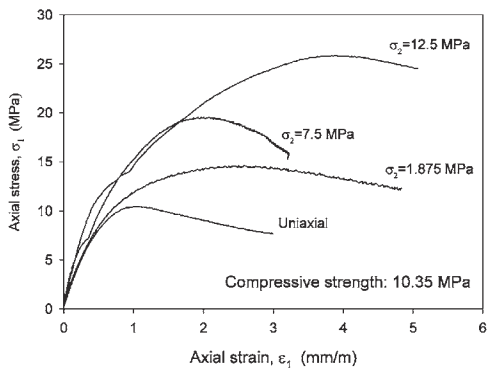


Figure 5 – Axial stress-strain relationship for low-strength concrete (G10) under lateral confinement

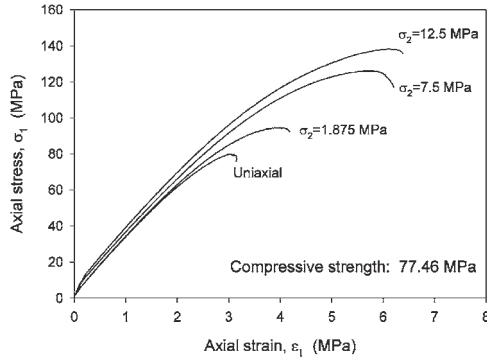


Figure 6 – Axial stress-strain relationship for high-strength concrete (G80) under lateral confinement

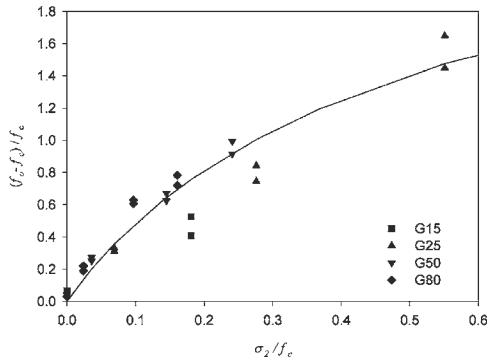


Figure 7 – Effect of compressive strength on the proposed failure envelope

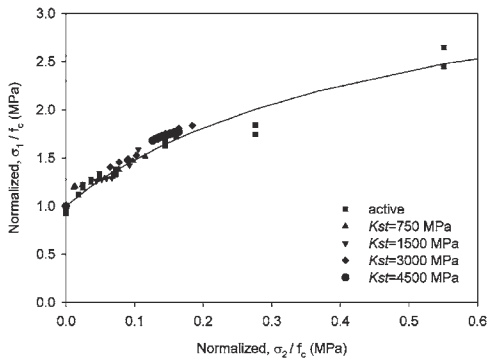


Figure 8 – Effect of stress path on the proposed failure envelope